

Production and morphological characterization of low resistance polyimide/silver nanowire nanocomposites: potential application in nanoconductive adhesives

Mehdi Hatami¹

Received: 1 August 2016 / Accepted: 1 November 2016 / Published online: 8 November 2016
© Springer Science+Business Media New York 2016

Abstract A new generation of polyimide (PI)/silver nanowires nanocomposites were prepared by a solution mixing method with different contents of prepared silver nanowires. The structural and properties of pure PI and PI/Ag nanocomposites were studied by several techniques such as fourier transform infrared spectroscopy (FT-IR), nuclear magnetic resonance spectroscopy, field emission scanning electron microscopy (FE-SEM), atomic force microscopy (AFM), X-ray diffraction (XRD), electrochemical impedance spectroscopy, and thermal analyses. FT-IR and ¹H-NMR spectra confirmed the success in preparation of PI sample. The FE-SEM and AFM analyses show the good dispersion of silver nanostructure in the PI matrix. The XRD pattern shows the presence of crystalline nature of inorganic silver nanowires in the organic amorphous PI matrix. The thermal and impedance spectroscopy analyses results reveal that, with increases in the content of silver in PI matrix up to the 2 vol%, the conductivity, and thermally stability factors of samples were increased.

1 Introduction

Aromatic polyimides (PIs), as thermally stable polymers, have displayed a series of outstanding characteristics, such as excellent thermo-stability, mechanical and dielectric properties. PIs are widely used in microelectronic, aerospace engineering, and other modern industries [1–3]. However, the technological and industrial applications of

rigid PIs are limited by processing difficulties, due to their high melting or glass transition temperatures and lack of solubility in most organic solvents [4]. Nowadays by increasing the demand for high technological material the application of different derivatives of PIs are greater than before [5]. The composites of PIs with different nanostructure materials were introduced in recent years. Incorporation of inorganic materials in PI matrices can improve the mechanical, thermal, dielectric and optical properties of PIs [5–8]. Thus, the obtained nanocomposites can combine the properties of PIs and inorganic materials, and the resultant properties are different than that of constituents [9]. In recent years, various nanosize inorganic components with high surface area have been used to enhance the performance of PI matrices [10–12]. Faghihi et al. [10] reported the preparation of PI/silver nanocomposites by in situ polymerization of diamine with dianhydride in the presence of silver ions as the silver sources, to lead the fabrication of nanocomposites with well dispersion properties. Different bifunctional organic and inorganic molecules, as starting materials have recently been used to prepare PI nanocomposites with improved mechanical, thermal and other properties by incorporation of inorganic components into the prepared PI matrices [10, 11]. Therefore, the inorganic nanostructures as fillers is one of the effective methods that improve the mechanical and thermal properties of the polymer matrix, which formed the network of organic–inorganic material in the form of nanocomposites [12]. Among the different nanostructure of the silver the Ag nanowires have attracted much attention due to their important applications in different scientific areas such as sensors [13, 14], inks [15], and other modern industries [16–18]. For preparation of silver nanostructures various methods have been assumed [19–21]. Ag nanostructures were prepared in different states including silver

✉ Mehdi Hatami
Hatami@bonabu.ac.ir

¹ Polymer Research Laboratory, Department of Polymer Science and Engineering, University of Bonab, Bonab, Iran

nanoparticles, nanowires, nanorods, nanoplates, and dendrite structure [21–24]. Among the different fabrication methods of silver nanostructures, the chemical reduction of silver ions to silver metals based on different reducing agents such as the polyol [25] process, which is suitable, adaptable and low costing process were applied to the synthesis of silver metal nanostructures. By varying the fabrication items in the synthesis complex, all kinds of structures with dissimilar morphologies can be obtained.

The performance of the poly(amic acid) and PI in nanotechnology was mainly related to the nanocomposite sciences. The poly(amic acid)s are the intermediate structures for PIs [4]. The poly(amic acid)s were converted to the PIs by chemical or thermal procedures. Actually poly(amic acid)s easily processed rather than PIs. For application in nanocomposite science the applications were depended on to the adhesion strength between the dispersed nanoscale materials and the continuous poly(amic acid) or PI phases. In comparison of poly(amic acid)s and PIs, due to the better physical and mechanical properties of PIs than poly(amic acid)s the applications of PIs were enhanced in nanocomposite sciences.

To best of our knowledge, there are only a few papers for evaluation of conductive properties of synthetic PI and silver nanowires for application in nanoconductive adhesives were published [26]. Other publication papers were described the insertion of nanowire or mixed nanowire and organic carbon containing structures as the conductive materials [27–29]. Therefore, this is the first report for preparation of synthetic PI with pendant benzamide units applied in conductive materials in the presence of silver wires in nanoscale level.

The main objective for this study was to fabrication of high thermally stable and low resistance PI/silver nanocomposites. Therefore, we synthesized PI containing preexisted amide and ester units in the side chains and imide units in the main chains of macromolecules by especial modified one pot chemical method for the first time. The prepared PI was used in structure of nanocomposites by announced the novel PI matrix in the presence of silver nanowires as a novel conductive structure with potential application area in adhesive, sensors, inks and circuit boards industries. The presence of amide and ester units in the side chains of polymer could help the nanowire to well orient in the matrix composition and provided better compatibility between organic and inorganic phases. Due to the undoubted effects of functional units in the stabilization of silver nanowires in preparation stage, insertion of polymer with special designed functional units certainly stabilized the nanowire in nanocomposites and provided better performances for fabricated samples.

2 Experimental

2.1 Materials

All the reagents were purchased from Aldrich and Merck chemical Co. and used without further purification. *N,N*-dimethylacetamide (DMAc), and *N*-methyl-2-pyrrolidone (NMP) were dried over BaO, then distilled in vacuum.

2.2 Equipments

Infrared spectra of the samples were recorded at room temperature in the range of 4000–400 cm^{-1} , on FT-IR Rayleigh (WQF-510) spectrophotometer. The spectra of solids were obtained using KBr pellets. The vibrational transition frequencies are reported in wavenumbers (cm^{-1}). Band intensities are assigned as weak (w), medium (m), strong (s) and broad (br). The (^1H -NMR, 500 MHz) spectrum was recorded by using a Bruker (Germany) DRX-600 instrument at room temperature in dimethylsulphoxide- d_6 (DMSO- d_6). Multiplicities of proton resonance were designated as singlet (s), doublet (d), and multiplet (m). Inherent viscosities were measured by a standard procedure using a Cannon–Fenske routine viscometer (Germany) at the concentration of 0.5 g/dL at 27 °C. Thermogravimetric analysis (TGA) is performed with a Mettler TA4000 at a heating rate of 10 °C/min from 25 to 800 °C under nitrogen atmosphere. The XRD pattern was acquired by using a D $_8$ ADVANCE, Bruker. The diffractograms were measured for 2θ , in the range of 10–80°, using Cu K α incident beam ($\lambda = 1.51418 \text{ \AA}$). The dispersion morphology of the nanostructures on PI matrix was observed using field emission scanning electron microscopy [FE-SEM, HITACHI (S-4160)]. AFM topographic pictures were obtained using digital multimode instruments Compact Frame, Bruker. A transmission electron microscope (ZEISS EM900 operating at 50 kV) was used to observe the morphology of nanocomposites

2.3 Polymer synthesis

According the synthesis of PI typically was carried out as follows: A 50-mL, one-necked, round-bottomed flask equipped with a magnetic stirrer, with 2 mmol of the 5,3-amino-*N*-(4-hydroxy phenyl)benzamide and 10 mL of dry NMP. The mixture was stirred at 0 °C for 0.5 h then 2 mmol of Benzophenone-3,3',4,4'-tetracarboxylic dianhydride (BTDA) was added and the mixture was stirred at 0 °C for 1 h. The temperature was raised to room temperature and the solution was stirred for 24 h. Poly(amic acid) was precipitated by pouring the flask content into 200 mL of a 3:1 volume mixture of water and methanol.

Then it was filtered, washed with hot water and dried under vacuum at 60 °C for 24 h. (Yield 91%).

Chemical cyclization was applied for conversion of poly(amic acid) to PI. Into a 50-mL, two-necked, round-bottomed flask equipped with a magnetic stirrer, nitrogen gas inlet tube, and a reflux condenser was placed 0.25 g of poly(amic acid) and 5 mL of dry NMP. The mixture was stirred and then 5 mL of acetic anhydride and 15 mL of pyridine were added. The mixture was stirred for 0.5 h and then slowly heated to 140 °C and held for 6 h at the same temperature. After that the mixture was cooled and poured into water, it then was filtered, washed with hot water and methanol, and dried under vacuum at 60 °C for 24 h (Yield 90%).

2.4 Synthesis of silver nanowires

Silver nanowires were fabricated using the polyol reduction procedure of silver nitrate (AgNO_3) in the presence of polyvinylpyrrolidone (PVP) as a polymeric surfactant in order to stabilization and prevention of the aggregation of the silver nanostructures as described by different scientific reports [30–32]. In a typical synthesis procedure, 100 mL of ethylene glycol were heated up 180 °C under vigorous magnetic stirring and the 2.93 g of PVP (Mw 55000) were added to the completely dissolved. After that the solution was cooled down gradually to ambient temperature. A exact 0.79 g powdered of silver nitrate, 0.5 mL of an aqueous solution of CuCl_2 (containing 0.03 g CuCl_2), and 5 mL of ethylene glycol were stepwise inserted to the PVP solution. The prepared solution was warmed from ambient temperature to 180 °C at a gradient of 2.5 °C/min under moderate stirring (100 rpm). The reaction was maintained at 180 °C for a further 3 h from starting the procedure, and was finished by gradually decreased the reaction temperature to room temperature. An amount of 30 mL of prepared sample solution was then mixed with 40 mL isopropyl alcohol followed by centrifugation at 9000 rpm for 4 min. Subsequently the supernatant were removed and then to redisperse the precipitate the 40 mL isopropyl alcohol was added and the dispersion was centrifuged at 9000 rpm for 4 min. The obtained precipitate was again dispersed in 5 mL *N,N*-dimethyl formamide (DMF) for forthcoming application.

2.5 Fabrication of the PI/silver nanowire nanocomposites

In the first step proper amounts of PI was dissolved in 10 mL DMF. A clear solution was obtained after stirring at 70 °C for 8 h. Appropriate amounts of homogenized silver nanowires using a sonicator (ultrasonic homogenizer, The Ultrasonic Tech. Development Co. (UTDC), Iran) were

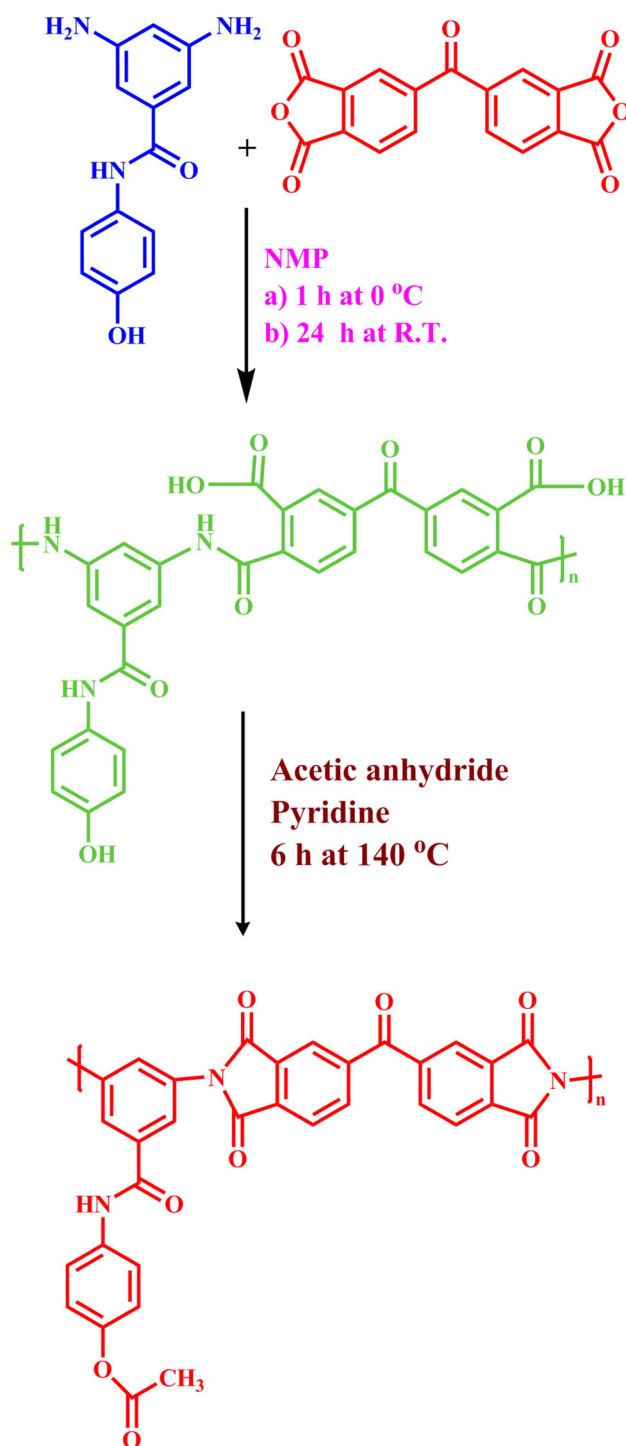
weighted. In the second step the suspension of Ag nanowire was then added and combined with the proper amount of silver nanowires. The resulting blend was sonicated for 4 h to guarantee the good dispersion of the silver nanowires in polymer solution. The final solution was casted into aluminum plates under vacuum, and finally left in a fume hood for 1 week to permit the completely evaporation of the solvent form the nanocomposite films. The silver nanowires loading levels in the PI film were 0.5, 1, 1.5, and 2% (volume percentage relative to PI). The prepared samples were assigned as NC1, NC2, NC3, and NC4 accordingly.

3 Results and discussion

3.1 FT-IR and $^1\text{H-NMR}$ characterizations

In this study PI was synthesized in two steps. In the first step by low temperature reaction of the diamine [33] with BTDA the poly(amic acid) was prepared [34]. In the second step by chemical imidization process the PI structure was performed. Although in the common process of conversion of the poly(amic acid) to PI only the five membered ring was created, but due to the presence of phenolic hydroxyl unit on the side chain of the polymer, the structure of poly(amic acid) and related PI was completely different. This is not a common process in the conversion of poly(amic acid) to chemically modified PI structure. The functional poly(amic acid) containing phenolic groups were acetylated by using acetic anhydride as a starting materials for chemical imidization process. This functionalization caused to change in the nature of the prepared polymer matrix. The presence of hydroxyl unit in the side chain of the poly(amic acid) were increased the hydrogen bonds between the polymeric chains. By thermal imidization process the assumed PI showed very rigid structure due to the unflexibility of the main chain and the many hydrogen interaction on the side chains. By elimination of the hydroxyl units the strong hydrogen bonds between the polymer functional units were decreased. Formation of acetyl groups on the side chain of the polymer modified the PI structure. The preparation procedure for the synthesis of PI was shown in scheme 1.

The chemical structure of poly(amic acid), and PI were characterized by FT-IR analysis technique. The characteristic imide absorption bands at 1778 cm^{-1} (imide C=O, symmetric stretching), 1713 cm^{-1} (imide C=O, asymmetric stretching), 1392 cm^{-1} (C–N stretching) and 721 cm^{-1} (imide ring deformation) were observed in all prepared samples. The characteristic amide peaks for poly(amic acid) was appeared at 1668–1664 cm^{-1} (amide-I band, C=O stretching), 1562 cm^{-1} (amide-II band, interaction



Scheme 1 The preparation procedure for the synthesis of PI

between NH deformation and C–N stretching). Due to the presence of amide unit in the structure of diamine and also in the preparation of poly(amic acid), after the chemical cyclization of amic acid units and the creation of imide units, the absorption peaks of the amido group were not fully faded. The poly(amic acid) and PI structures also were characterized by $^1\text{H-NMR}$ spectroscopy. The

chemical structure of poly(amic acid) and PI (Fig. 1) were confirmed by $^1\text{H-NMR}$ in $\text{DMSO-}d_6$. Two carboxylic protons of poly(amic acid) due to the ring opening of anhydride groups were became visible as a wide peak at 10.5–11.0 δ ppm. The phenolic groups connected to the side chain (bulky pendent unit) were shown as a sharp peak at 9.18 δ ppm. The poly(amic acid) aromatic protons were came into view as multiplets at 6.83–8.22 δ ppm. The signals at 9.80 and 9.65 ppm were assigned to the protons from NH groups of amide units presented from the benzamide structures and the new amide unit created from the reaction of the diamine and the dianhydride in poly(amic acid) structure. After the cyclization process, the characteristic peaks associated to the carboxyl, one of the amides, and hydroxyl units were disappeared. The new peaks with little displacement in chemical shifts to pre-existed proton peaks were shown, and in addition those, the acetyl units related to the acetylation process of phenolic hydroxyl unit showed characteristic peak at 2.17 ppm. Therefore, the $^1\text{H-NMR}$ spectra of prepared sample as well as the FT-IR technique data confirmed the synthesis of novel PI matrix.

The FT-IR analysis data related to the PI/silver NCs with different contents were collected in Table 1. Due to the existence of the different functional units such as amide, imide, ester, benzene ring, aliphatic and aromatic structures on the construction of PI, the absorption peaks of the silver nanowires were not obviously detectable. Also NCs peaks intensity gradually increased by increasing of silver nanowire stabilized by PVP contents and is an indication of the incorporation of silver nanowire stabilized PVP into the polymer matrix. These results revealed the success in synthesizing the Ag nanowire/PI NCs.

3.2 AFM investigations

The atomic force microscope (AFM) is well-established equipment in the materials science field of research. AFM was developed in 1985 as deploy of scanning tunneling

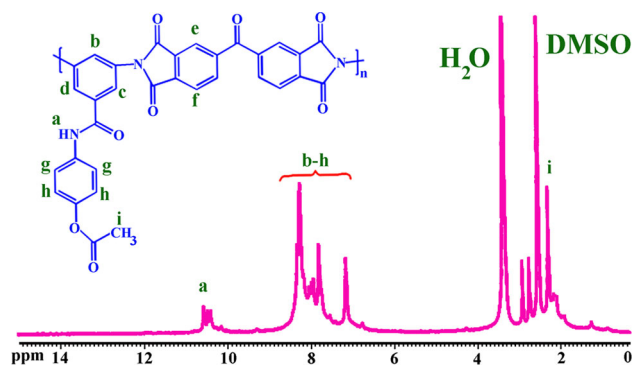


Fig. 1 Graphical illustration and analysis of $^1\text{H-NMR}$ spectrum for the PI structure

Table 1 Spectroscopic analyses results for nanocomposites based on FT-IR technique

	NC1	NC2	NC3	NC4
FT-IR (KBr, v _{max} /cm ⁻¹)	3864, 3743, 3617, 3280, 3064, 2994, 1778, 1727, 1660, 1600, 1511, 1451, 1363, 1189, 1089	3841, 3743, 3617, 3066, 2998, 1778, 1728, 1661, 1601, 1512, 1451, 1355, 1450, 1189	3843, 3743, 3662, 3619, 3281, 3058, 2972, 1778, 1729, 1660, 1602, 1511, 1445, 1351, 1188, 1088	3854, 3735, 3615, 3281, 30,564, 2927, 1779, 1727, 1661, 1601, 1516, 1455, 1350, 1188, 1081

microscopy. Case selected material can be imaged under ambient circumstances. Preparation route is relatively simple, and the AFM can be used to image both conducting and non-conducting compounds. AFM technology is still opening and has only lately been applied to material science troubles. The better understand in the morphological quantitative description of the nanostructure surface could be achieved by topographic investigation of the surfaces. The data related to the topographic analysis results could be obtained by the investigation of the two dimensional profile lines (2D) or over the total picture profiles by three dimensional explorations of the nanostructure surfaces (3D). Figure 2 illustrated the 2D and 3D AFM topography images of surface of the NC 1 with a scan size of 5 μm².

Among the different surface parameters the amplitude parameter could be categorized as a principal parameter in characterization of the surface topographic studies. The value for the average roughness (R_a) and the root mean square roughness (R_q) are the main height parameters used for study the surface profile. The average roughness (R_a) was defined as the following equation [35].

$$R_a(N, M) = 1/N \sum_{x=1}^N (z(x, y) - z(N^-, M))(2D) \quad (1)$$

$$R_a(N, M) = 1/NM \sum_{x=1}^N \sum_{y=1}^M (z(x, y) - z(N^-, M))(3D) \quad (2)$$

In the mentioned equations the zed bar was referred to the arithmetic average height value. The most common amplitude parameter (roughness) for evaluation of the

selected gate for prepared NC 1 sample are presented in Table 2, and was graphically observable at Fig. 3. The maximum height of the roughness was reported as (R_t). Similarly the R_t defined as a total roughness (R_t = R_v + R_p). R_p was defined as the maximum profile peak height. Also the R_v was known as the maximum profile valley depth.

The amplitude distribution function (ADF) is the functional parameter may provide quantitative information about the asymmetry and flatness of the surfaces. The third order of outline amplitude probability density function is defined as Skewness (R_{sk}) and is applied to the quantity evaluation of the symmetry of the profile from the mean line. In addition to R_{sk}, the Kurtosis (R_{ku}) moment is defined as a fourth moment of the probability function profile amplitude. R_{sk} and R_{ku} were applied to investigate the asymmetry and the surface sharpness or the grain structure distribution on the morphological aspects of the surfaces respectively. By analyzing the ADF and roughness curves given in Fig. 4, it could be observed that the surface height distribution and the surface roughness characteristics showed the unique concepts for this study. The value of the maximum roughness peak height (R_p) was measured 2.73 nm, and the maximum roughness valley depth (R_v) value was observed 2.34 nm. Therefore the ADF curve evidently showed the height distribution function for selected gate of the image. Also the R_t in roughness curve clearly observed by with comparing by the obtained results with ADF curve. The interrelationship of the functional parameters R_{sk} and R_{ku} with consideration to the NC composition is illustrated in Fig. 5. The valuation of the results for each NC denoted the grade of the symmetry of

Fig. 2 The 2D and 3D AFM topography images of surface of the NC 1 with a scan size of 5 μm²

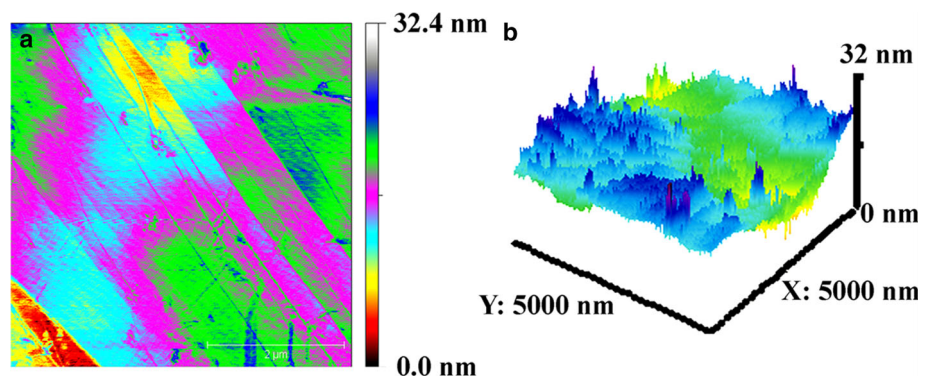
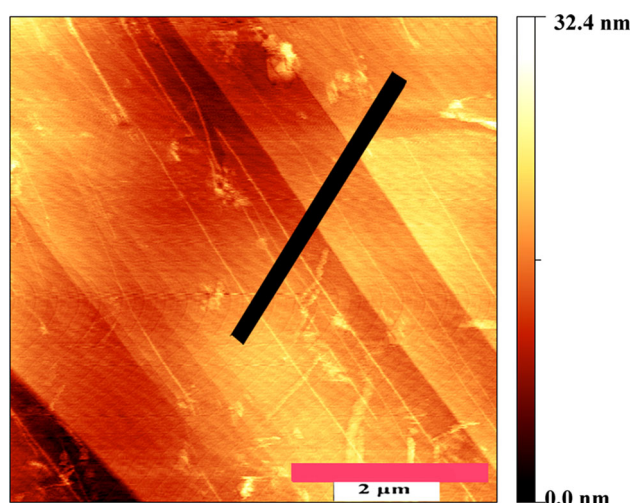


Table 2 Roughness parameters for NC1

Roughness parameters	Values (nm)
Roughness average (Ra)	0.53
Root mean square roughness (Rq)	0.69
Maximum height of the roughness (Rt)	5.07
Maximum roughness valley depth (Rv)	2.34
Maximum roughness peak height (Rp)	2.73
Average maximum height of the roughness (Rtm)	3.11
Average maximum roughness valley depth (Rvm)	1.44
Average maximum roughness peak height (Rpm)	1.67
Average third highest peak to third lowest valley height (R3z)	3.92
Average third highest peak to third lowest valley height (R3z ISO)	1.53
Average maximum height of the profile (Rz)	3.78
Average maximum height of the roughness (Rz ISO)	3.11

**Fig. 3** 2D image of NC1 with selected entry from AFM image

the surface height to the mean plane. R_{sk} is subtle to irregular valleys or high peaks. Therefore, the negative value for skewness was related to the more planar surfaces and the valleys are predominant in the surface structure. The R_{sk} value is positive, if the height distribution is asymmetrical, and the surface has more peaks than valleys. The negative R_{sk} obtained for NC1 shows the surface with shortened peaks or irregular deep valleys as understood in Fig. 5. The positive R_{sk} values, calculated by AFM software were achieved for three other samples, reveals shapes with special high peaks.

R_{ku} parameter was inspected since is expressive for representing the existence of defects either in form of valley or peak on the surface structure. The inferior positive values of the kurtosis suggested the very smooth surfaces and homogeneous structure. Also the obtained results indicated that the relatively uniform distribution of heights above and below the mean height was observed. When R_{ku} is equal to three indicating the gaussian amplitude

distribution, and the surface is called Mesokurtic. When the R_{ku} smaller than three the surface is flat and called Platykurtic. If the R_{ku} is higher than three, the surface has more peaks than valleys and called leptokurtic [36]. A distribution of the silver nanowire in PI matrix was observed and could be concluded by reflection of the small inorganic area on the surface of organic composites. The higher compatibility between the organic and inorganic segments was distinguishable and outstanding adhesion between inorganic and organic parts was obviously detected. In the selected slit there was not perceived main abruptness in the images. It can be concluded that nanostructures were dispersed in uniform mater in the NC structure and the surface investigation of the NC showed that the nano-parts with sizes <45 nm in few locations were observed. Figure 6 showed the images a, and b illustrated the edge detection presentation by local non-linearity and the step presentation of the Fig. 3 for NC 1 nanostructure. It appeared that with introducing the nano-materials in PI as the polymer matrix the hills of surface due to the presence of nanostructure in the surface were increased.

Several methods have been used to measure the fracture behavior of the surface. In this study a software Gwyddion package was used to analyze D from the AFM data. The basic quantitative component of fractal geometry, the fractal dimension D , is a non-integer number with a Euclidean and non-Euclidean component. The Euclidean component describes the topological dimension of the object, i.e., 1 for a line, 2 for an area or surface, and 3 for a volume. The non-Euclidean component, called the fractal dimensional increment, D^* , describes the level of irregularity of the object from its Euclidean geometry. The fractal dimensional increment ranges from 0 to 1, with the level of irregularity increasing as the increment increases. Several algorithms have been used to regulate the value of fractal dimension D constructed on the AFM data. In order to

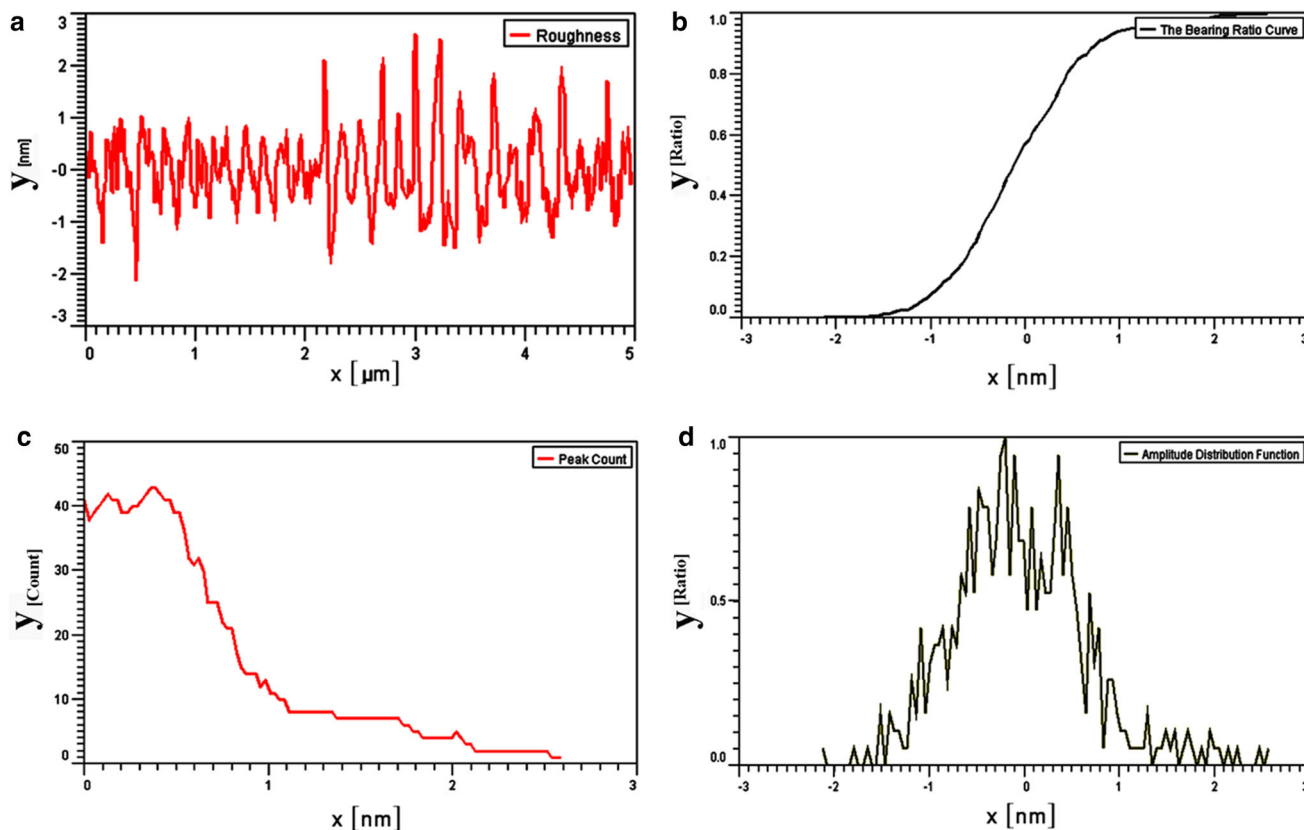


Fig. 4 Analyzing the roughness (a), bearing ratio (b), peak count (c), and ADF (d) curves

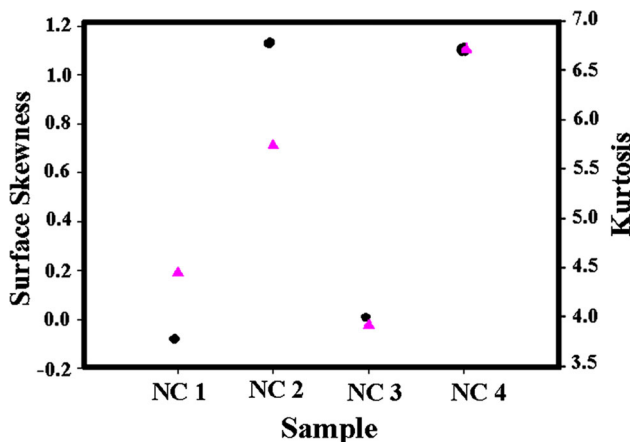


Fig. 5 Variation of the values of R_{sk} and R_{ku} with NC contents, (black circles for R_{sk} , and pink triangular related to the R_{ku} values) (Color figure online)

study the fractal features of silver NCs, to calculate D from the AFM data, a Gwyddion software package was used. Gwyddion is a free and open source software program for SPM data visualization and analysis [37]. Gwyddion uses four processes to compute D from AFM data: (I) cube counting, (II) triangulation, (III) variance and (IV) power spectrum distribution (Fig. 7). The average D^* values for the NC1 based on cube counting, triangulation, variance,

and power spectrum methods were 0.18, 0.23, 0.27, and 0.15 respectively. Fractal analysis has shown that all samples exhibit a self-similar character, which is concern to the fabrication route. Figure 7 illustrated the (a) power spectrum, (b) triangulation, (c) cube counting and (d) partitioning, and linear fit graphs for NC1.

3.3 X-ray diffraction patterns analysis

In the description of crystalline moieties in hybrid materials, estimation of the crystallite size is as important as the identification of the crystalline phase, elemental composition, and morphological explorations. The size of small particles in nano science could be considered by a number of experimental methods: dynamic light scattering (DLS), photon correlation spectroscopy (PCS), scanning electron microscopy (SEM), transmission electron microscopy (TEM), scanning probe microscopy (SPM), neutron diffraction (ND) and X-ray diffraction (XRD). Both XRD and TEM techniques permit synchronized determination of a crystallite size and a crystalline phase composition. Consequently, XRD is a regularly employed and current practice for the measurement of crystallite size. Figure 8 illustrates the XRD pattern of PI/silver nanocomposite NC4 as an example. On the pattern of nanocomposite a broad

Fig. 6 The edge detection presentation for NC1 from AFM image by local nonlinearity (a) and the step presentation (b)

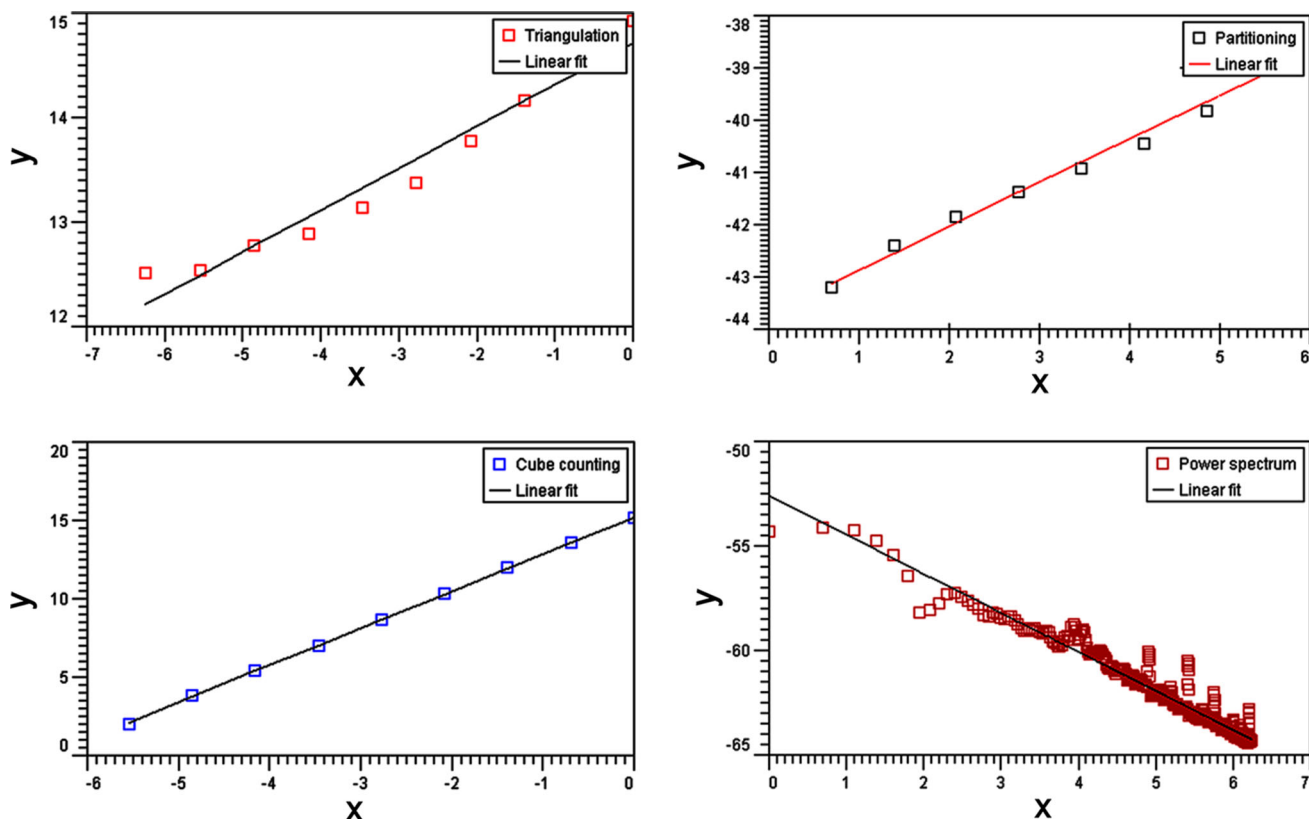
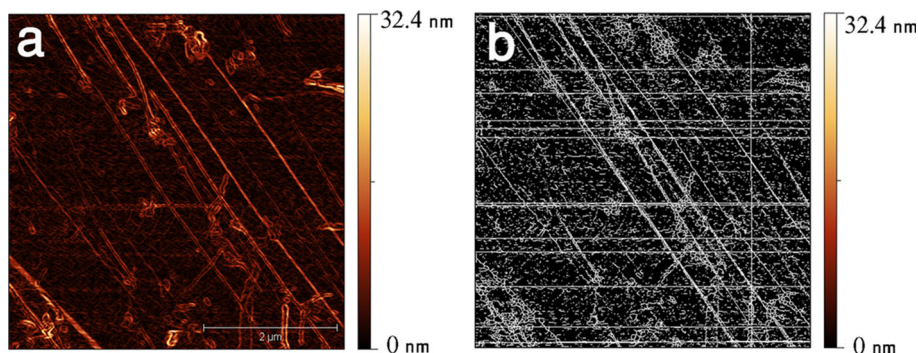


Fig. 7 Fractal analysis of NC1 by atomic force microscopy

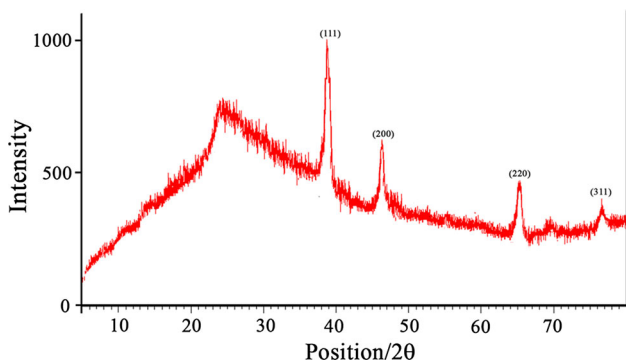


Fig. 8 XRD curve of NC3

peak in the range of $2\theta = 15\text{--}25^\circ$ was related to the PI matrix. The meaning of this broad band is that PI is amorphous. Also the XRD pattern was used to testify the existence, crystallite size, crystalline phase, and morphological explanation of the nanowires in the hybrid NCs. The XRD peaks, which correspond to the (111), (200), (220), and (311) at 2θ values of 38.2, 44.3, 64.5, and 77.5 related to the diffraction planes of silver were detected [38]. In the PI/silver nanocomposites, the diffraction peaks of nanostructure were unchanged. This points out that the silver nanowires remain stable after being inserted into the PI media. Also the XRD patterns for all samples showed the similar broadened patterns. For whole samples the good

agreement were observed for diffraction peaks for PI/Ag nanocomposite.

3.4 FE-SEM analysis of nanocomposites

Figure 9 shows the FE-SEM images of the neat PI and PI/silver nanocomposites with different amounts of nanostructures. The silver nanowire distributed relatively uniformly in the PI matrix. As can be seen, the silver nanowire

were good embedded in the PI matrix for the 1.5 vol% silver nanowire composite and showed good compatibility with PI, while for the neat PI sample, some arena were observed. However, the incorporation of nanowires can markedly change the morphology of the PI fractured surface. In addition, the smooth ribbon features which arise from the neat PI fracture surface diminished and evolved into smaller fragments. This can be ascribed to the induced crack because of the increases of free volume fraction at

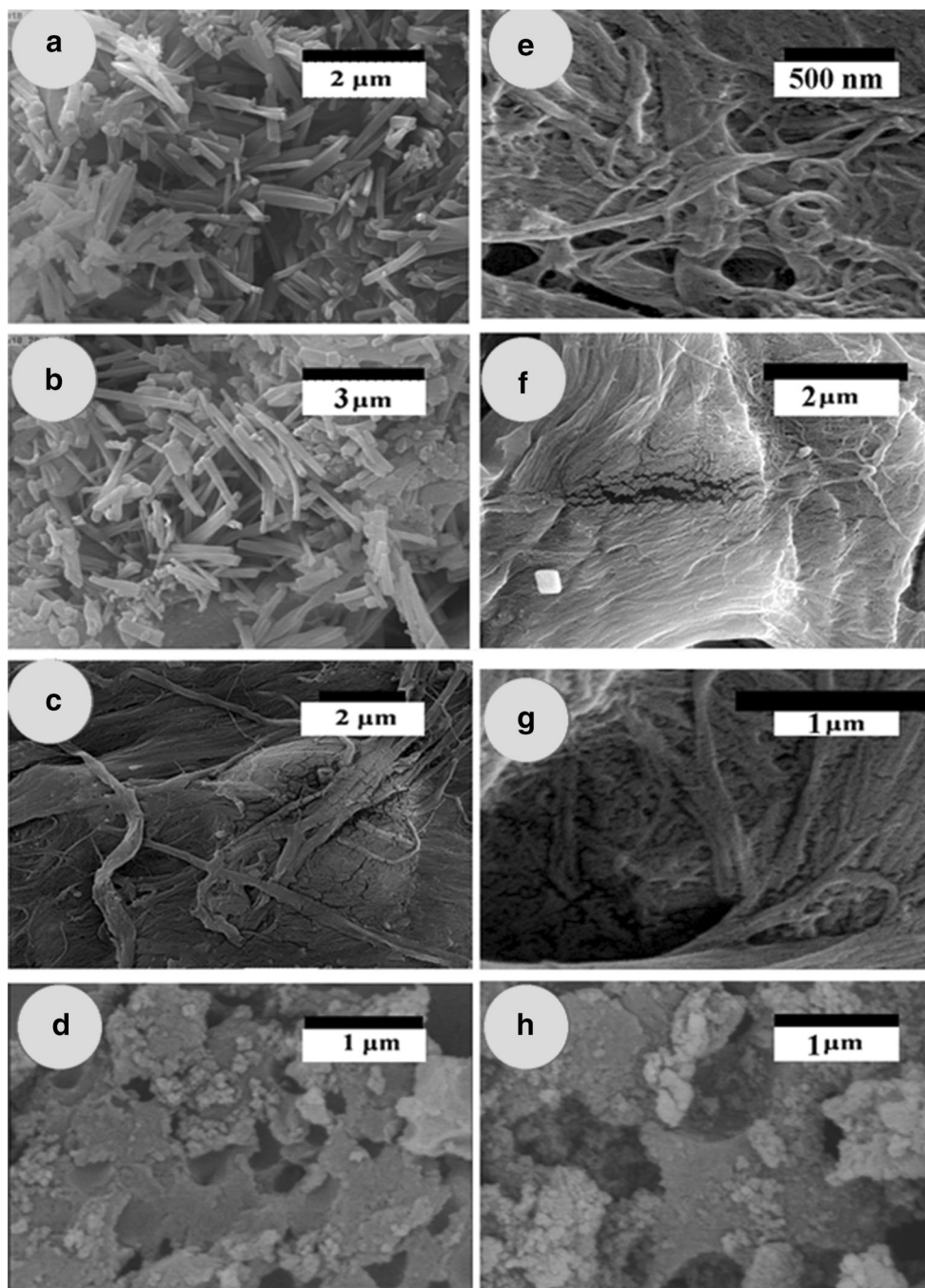


Fig. 9 FE-SEM micrographs of nanostructure (a, b), NC1 (c), NC2 (e), NC3 (f), NC4 (g), and PI (d, h)

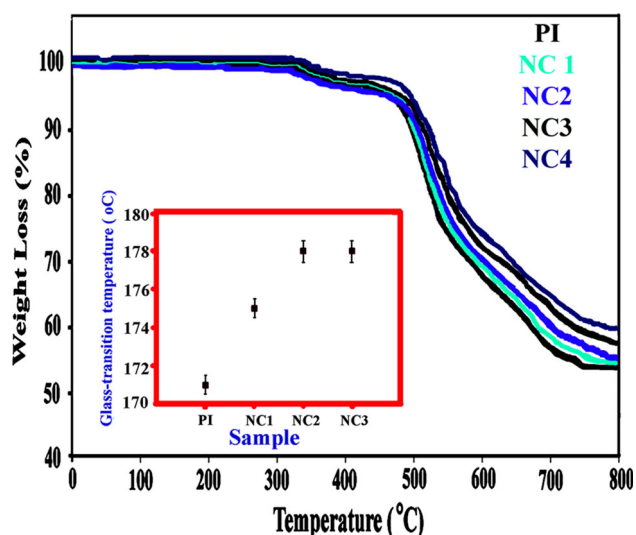


Fig. 10 TGA thermograms of PI, and NCs with different nanoscale contents under the nitrogen atmosphere at heating rate of 10 °C/min, also glass transition temperature was plotted as a function of NC sample in inserted picture

higher nanowire contents. It may be because of higher concentration of nanostructures, which was against forming percolated particle network and resulted in the change of the morphology of the nanocomposites. FE-SEM images demonstrated that the nanowires were well thought-out and homogeneously dispersed. It is understood that the formed networks between organic stabilized inorganic nanostructures and organic backbone of PI matrix can be considered as uniform composites. Functional groups of PI can form strong interaction with functional groups present on silver nanowires coverage. As a result, related interaction should develop the interfacial interaction between PI and nanosilver. In addition, the results illustrated that the structure of the prepared samples of NC 1 was more dense and uniform than other nanocomposites (Fig. 10).

3.5 Thermal analysis of PI NCs

The Thermal stability evaluation of the PI, and nanocomposites were carried out based on the degradation temperature of 5% weight loss (T_5) and the degradation

Table 3 Thermal properties of the PI and NCs

Sample	T_0 (°C)	T_5 (°C)	T_{10} (°C)	T_{max} (°C)	Char yield at 800 °C (%)
PI	281	439	489	521	54
NC1	284	441	494	529	56
NC2	287	448	499	547	56
NC3	287	453	502	550	58
NC4	289	453	520	550	60

Temperature at which 0, 5 and 10% weight loss and T_{max} was recorded by TGA at heating rate of 10 °C min⁻¹ in a N₂ atm

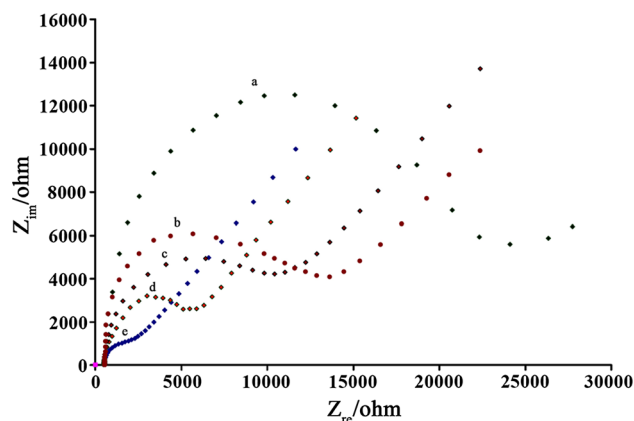


Fig. 11 The electrochemical impedance plots for **a** carbon paste electrode modified with PI, **b–e** carbon paste electrode modified with NC1–4 containing nanostructure silver in 1.0 mM [Fe(CN)₆]^{3-/4-} (1:1) solution in 0.1 M KCl

temperature of 10% weight loss (T_{10}) of the NCs by TGA analysis and the results are summarized in Table 3. The value of T_5 for prepared PI was measured around 451 °C and T_{10} value was estimated above 480 °C. The temperature of 5 and 10% weight loss and also the char yield at 800 °C of PI–silver nanocomposite were higher than the pure PI. The residual weight for the NC2 at 800 °C ranged in 54% in nitrogen atmosphere. According to TGA results, the thermal degradation behaviour of NCs with different percentages showed one major weight loss steps when they were heated from room temperature to 800 °C. The higher thermal stability of NC can be attributed to the presence of inorganic silver nanostructure into the PI matrix.

3.6 Conductivity analysis

Electrochemical impedance spectroscopy is a high performance and powerful technique for investigation of electrical conductivity of electroactive materials and especially nanoparticles at the electrode–solution interface [39].

The effects of synthesized Ag nanowire on electrical conductivity were investigated using electrochemical impedance spectroscopy (EIS) method. Electron transfer resistance, R_{ct} , is an important factor for this goal. The

semicircle portion at higher frequencies corresponded to the electron transfer limited process for a conductive surface or electroactive compound. Figure 11 shows the impedance plots for (a) carbon paste electrode modified with PI, (b–e) carbon paste electrode modified with NCs in 1.0 mM $[\text{Fe}(\text{CN})_6]^{3-/4-}$ (1:1) solution in 0.1 M KCl, respectively. It is evident from the EIS data that with increasing fraction value of Ag nanowire at a surface of carbon paste electrode, the value of electron transfer resistance decrease. Also, the R_{ct} for carbon paste electrode modified with PI is higher value than compare to carbon paste electrode modified with Ag nanowire that show PI is nonconductive compound and reduce electrical conductivity carbon paste electrode in the presence of $[\text{Fe}(\text{CN})_6]^{3-/4-}$ as a standard redox sample. On the other hand, we can be seen, the best electrical conductivity obtained in the presence of Ag nanowire at a NC4 and after of it the value of R_{ct} is constant (not shown).

4 Conclusions

A series of PI/Ag nanocomposites with various contents of Ag nanowires have been prepared by a solution mixing technique. The structure of the PI/Ag nanocomposites was studied by using XRD, FTIR, FE-SEM, and AFM analyses. The results of the XRD, FTIR, FE-SEM, and AFM indicated that the Ag nanowires distributed uniformly in polymer matrix. Pure PI showed amorphous structure and prepared nanocomposites showed a crystalline nature of silver nanowire and amorphous polymer pattern combinations. The results of AFM images represent the patterns of peaks and valleys due to the distribution of the Ag nanowires in the body and the surface of polymer matrix. TGA of nanocomposites denotes the increases in thermal factors with enrichment in the contents of inorganic nanostructure in nanocomposite samples. Morphological investigations using FE-SEM proved the patterns of ribbon like structure from the interactions of nanowires and PI matrix. These structures were provided due to the interaction of polymer functional units and the nanowires which were positioned between the macromolecular chains. Also the stabilization effects of polymer functional units caused to better cohesion of nanowires and organic matrix as were shown in FE-SEM images. The data obtained from FT-IR spectroscopy were shown the existence of characteristic absorption bands related to polymer and silver stabilized by PVP in the nanocomposite structures. Bolstering of PI with silver nano fillers increase the physical and chemical properties of the prepared films and expand the applications of them. This hybrid material can be used in different industrial fields such as electrical conductive adhesives.

Acknowledgements The author gratefully acknowledge Iran National Science Foundation (INSF) for support of this work under Project No. 91054935 and University of Bonab, Bonab, and also Khoramshahr Marine Science and Technology University, Khoramshahr, Iran for their cooperation.

References

1. P.E. Cassidy, *Thermally Stable Polymers* (Marcel Dekker, New York, 1980), pp. 15–56
2. D. Wilson, H.D. Stenzenberger, P.M. Hergenrother, *Polyimides* (Blackie, London, 1990), pp. 34–46
3. M.I. Bessonov, V.A. Zubkov, *Polyamic Acids and Polyimides: Synthesis, Transformations, and Structure* (CRC Press, Boca Raton, 1993), pp. 201–218
4. V. Mittal, *Thermally Stable and Flame Retardant Polymer Nanocomposites* (Cambridge University Press, New York, 2011), pp. 121–138
5. J. Njuguna, *Structural Nanocomposites: Perspectives for Future Applications* (Springer, Heidelberg, 2013), pp. 173–184
6. B.N. Nguyen, E. Cudjoe, A. Douglas, D. Scheiman, L. McCorkle, M.A.B. Meador, S.J. Rowan, *Macromolecules* **49**, 1692 (2016)
7. S.-K. Kim, T. Liu, X. Wang, *A.C.S. Appl. Mater. Interfaces* **37**, 20865 (2015)
8. Y. Qin, Q. Peng, Y. Ding, Z. Lin, C. Wang, Y. Li, F. Xu, J. Li, Y. Yuan, X. He, Y. Li, *ACS Nano* **9**, 8933 (2015)
9. H. Zhou, W. Yu, C. Qu, C. Liu, D. Wang, *J. Mater. Sci.: Mater. Electron.* **26**, 9789 (2015)
10. K. Faghihi, M. Hajibeygi, *J. Saudi Chem. Soc.* **17**, 419 (2013)
11. N.V. Kamanina, S.V. Serov, N.A. Shurpo, S.V. Likhomanova, D.N. Timonin, P.V. Kuzhakov, N.N. Rozhkova, I.V. Kityk, K.J. Plucinski, D.P. Uskokovic, *J. Mater. Sci.: Mater. Electron.* **23**, 1538 (2012)
12. A. Ahmad, H. Wu, Y. Guo, Q. Meng, Y. Meng, K. Lu, L. Liu, Z. Wei, *RSC Adv.* **6**, 33287 (2016)
13. P. Knauth, J. Schoonman, *Nanocomposites: Ionic Conducting Materials and Structural Spectroscopies* (Springer, New York, 2008)
14. M. Amjadi, A. Pichitpajongkit, S. Lee, S. Ryu, I. Park, *ACS Nano* **8**, 5154 (2014)
15. W. Yang, C. Liu, Z. Zhang, Y. Liu, S. Nie, *J. Mater. Sci.: Mater. Electron.* **24**, 628 (2013)
16. D.-G. Kim, J. Kim, S.-B. Jung, Y.-S. Kim, J.-W. Kim, *Appl. Surf. Sci.* **380**, 223 (2016)
17. C.-Y. Lin, D.-H. Kuo, W.-C. Chen, M.-W. Ma, G.-S. Liou, *Org. Electron.* **13**, 2469 (2012)
18. Y. Kim, J.-W. Kim, *Appl. Surf. Sci.* **363**, 1 (2016)
19. Y. Tang, W. He, S. Wang, Z. Tao, L. Cheng, *J. Mater. Sci.: Mater. Electron.* **25**, 2929 (2014)
20. S. Wang, Y. Tian, S. Ding, Y. Huang, *Mater. Lett.* **172**, 175 (2016)
21. A. Jeevika, D.R. Shankaran, *J. Colloid Interface Sci.* **458**, 155 (2015)
22. Y. Mao, C. Wang, H. Yang, *Mater. Lett.* **142**, 102 (2015)
23. K. Jia, H. Shou, P. Wang, X. Zhou, X. Liu, *Appl. Surf. Sci.* **377**, 180 (2016)
24. B. Rezaei, S. Damiri, *Talanta* **83**, 197 (2010)
25. J.-Y. Lin, Y.-L. Hsueh, J.-J. Huang, J.-R. Wu, *Thin Solid Films* **584**, 243 (2015)
26. H. Wang, D. Zhu, W. Zhou, F. Luo, *Ind. Eng. Chem. Res.* **54**, 6589 (2015)
27. N. Atar, E. Grossman, I. Gouzman, A. Bolker, V.J. Murray, B.C. Marshall, M. Qian, T.K. Minton, Y. Hanein, *ACS Appl. Mater. Interfaces* **7**, 12047 (2015)

28. J. Lim, H. Yeo, M. Goh, B.C. Ku, S.G. Kim, H.S. Lee, B. Park, N.H. You, *Chem. Mater.* **27**, 2040 (2015)
29. M. Yoonessi, J.R. Gaier, J.A. Peck, M.A. Meador, *Carbon* **84**, 375 (2015)
30. A. Gomez-Acosta, A. Manzano-Ramirez, E.J. Lopez-Naranjo, L.M. Apatiga, R. Herrera-Basurto, E.M. Rivera-Munoz, *Mater. Lett.* **138**, 167 (2015)
31. S. Coskun, B. Aksoy, H.E. Unalan, *Cryst. Growth Des.* **11**, 4963 (2011)
32. Y. Sun, B. Mayers, T. Herricks, Y. Xia, *Nano Lett.* **3**, 955 (2003)
33. S. Mallakpour, M. Hatami, *Des. Monomers Polym.* **14**, 461 (2011)
34. S. Yazdani, M. Hatami, S.M. Vahdat, *Turk. J. Chem.* **38**, 388 (2014)
35. P. Eaton, P. West, *Atomic Force Microscopy* (Oxford University Press Inc., New York, 2010), pp. 25–76
36. X. Xue, L.M. Phinney, A.A. Polycarpou, *Microsys. Technol.* **14**, 17 (2008)
37. Necas, D., Klapetek, P.: Gwyddion—free SPM (AFM,SNOM/NSOM, STM, MFM, ...) data analysis software. <http://gwyddion.net/>. Accessed 01 Feb 2016
38. D. Zhang, L. Qi, J. Yang, J. Ma, H. Cheng, L. Huang, *Chem. Mater.* **16**, 872 (2004)
39. D. Sotta, J. Bernard, V. Sauvant-Moynot, *Prog. Org. Coat.* **69**, 210 (2010)